Complete Characterizations of Intermediate and Final State Wave Functions with Photoionization of Polarized Rb

Huanyu Ma,[1,2,*] Linxuan Zhang,[3,4,*] Xincheng Wang,[1,†] Zhihan Zou,[1,2] Rujin Lv,[2] Zhenjie Shen,[1] Ahai Chen,[1] Matthias Weidemüller,[5] Kiyoshi Ueda,[1] Difa Ye,[3,‡] and Yuhai Jiang[1,2,6,§]

[1]*Center for Transformative Science and School of Physical Science and Technology, ShanghaiTech University, Shanghai 201210, China*

[2]*Shanghai Advanced Research Institute, Chinese Academy of Sciences, Shanghai 201210, China*

[3]*National Key Laboratory of Computational Physics, Institute of Applied Physics and Computational Mathematics, Beijing 100088, China*

[4]*Graduate School, China Academy of Engineering Physics, Beijing 100193, China*

[5]*Physikalisches Institut, Universität Heidelberg, Im Neuenheimer Feld 226, 69120 Heidelberg, Germany*

[6]*School of Physics, Henan Normal University, Xinxiang 453007, China*

(Received 3 August 2024; revised 16 December 2024; accepted 7 March 2025; published 27 March 2025)

The amplitude and phase of a photoionization channel provide deep insights into the nature of ionization dynamics. Here, we propose a novel experimental approach to retrieve these parameters from the photoelectron momentum distribution (PMD), where a 400 nm femtosecond laser is used to ionize polarized Rb atoms prepared in the $5p$ state. The magnetic quantum numbers of polarized atoms are well controlled by breaking down the symmetry of the cooling laser in a magneto-optical trap reaction microscope. From the tilt angle of the PMD and the interference structure of ϵs and ϵd ionization channels, we are able to extract their relative amplitude and phase shift, in good agreement with *ab initio* calculations. This exhibits a benchmark one-photon single ionization study of the hydrogen-like atom, providing a *complete* measurement with full characterizations of intermediate and final state wave functions.

DOI: 10.1103/PhysRevLett.134.123204

Photoionization is a fundamental process for understanding light interaction with matter and can be clearly described in the energy domain according to Einstein's explanation of the photoelectric effect. What is less clear is how long the photoelectric effect actually takes [1,2]. It is known the photoionization time delay mainly arises from the energy-dependent scattering phase shift that occurs during an electron escaping out of the atomic potential, coined as the Eisenbud-Wigner-Smith (EWS) time delay [3–5]. To fully understand the photoionization dynamics, a *complete* measurement is necessary, requiring the determination of the amplitudes and relative phases of different ionization channels [6,7].

Synchrotron radiation, in particular the availability of short wavelength sources, has facilitated the *complete* measurements of photoionization processes since the 1970s [8], although the standard procedure is quite tedious. There, in addition to the measurements of the partial photoionization cross section and the angular distribution, other physical quantities such as the spin polarization [9,10] or the fine structure of Auger transition in the residual ion [11] are also required to reach a *complete* reconstruction of the photoionization dynamics. Alternatively, a resonant prepulse is often combined with the synchrotron radiation to prepare excited states with a specific alignment or orientation, leading to magnetic dichroism and phase tilt that can be utilized to extract the information. These experiments mainly concentrate on resonant photoionization processes of inner-shell electrons, necessitating the consideration of spin-orbit coupling effects [12–17]. Subsequent Auger or fluorescence decay might get entangled in the *complete* measurements. Moreover, since most of the experiments were performed with noble-gas atoms or alkaline-earth metals, electron-correlation effects such as the Fano resonance might complicate the theoretical interpretation [18].

With the development of ultrafast science into the realm of attoseconds [19,20], the phase information of electronic transitions can be obtained through attosecond metrology [21], such as the attosecond streak camera [22,23] and the reconstruction of attosecond beating by interference of two-photon transitions (RABBIT) technique [24–26]. In these pump-probe schemes, the requirement of a second laser pulse introduces complexity to the measurement, as the interaction with the probing field adds an extra phase and projects the electron wave packet to other partial waves,

*These authors contributed equally to this work.
†Contact author: wangxch1@shanghaitech.edu.cn
‡Contact author: ye_difa@iapcm.ac.cn
§Contact author: jiangyh3@shanghaitech.edu.cn

making the characterization of the original single-photon ionization more complex and failing to provide the amplitude ratios [27].

In this Letter, we use a state-of-the-art in-house experimental setup, so-called MOTReMi [28,29], which is a combination of the magneto-optical trap (MOT) and a reaction microscope (ReMi), to perform one-photon single ionization of the well-controlled initial polarized state and achieve *complete* measurements. The single-active-electron approximation is valid for Rb atoms, thus permitting a very straightforward comparison between experiment and theory. Moreover, relativistic effects such as spin-orbit coupling are negligible as verified in previous work [29]. In this sense, it provides the simplest and cleanest benchmark test for *complete* studies. The laser cooling technique allows preparing the Rb atoms in an excited state ($5p$) with highly controllable alignment and orientation, where one can control the magnetic quantum number m of the excited Rb atoms by keeping only a single beam of cooling laser. By creating such a well-characterized intermediate state, which serves as the initial state of the photoionization process, we can fully reconstruct the subsequent dynamics of single-photon ionization without the intervention of another probing light.

In our experiment, the wavelength of the cooling laser used in the MOT is 780 nm, nearly resonant with the transition between the ground state $5s$ and the excited state $5p$ (spin-obit coupling effects are very weak and thus can be safely neglected throughout the Letter [30]) of the Rb atom, so these two states coexist in our setup. The proportion of $5p$ state is about 20% according to our early measurements and calculations [29]. The six cooling laser beams are left-handed circularly polarized. Therefore, the excited Rb atoms are populated into a Zeeman sublevel with the magnetic quantum number $m = 1$, which means they are also polarized into six different directions, corresponding to the propagation direction of each cooling laser beam shown in Fig. 1(a) by the red arrows. For the ionizing laser, the fundamental field (800 nm, 35 fs, 1 kHz), generated by a Ti:sapphire laser system, is frequency doubled with a β-barium-borate crystal to produce its second harmonic (400 nm). The laser intensity is adjusted by a $\lambda/2$ wave plate and a thin-film polarizer, and the ellipticity of the laser field is controlled using a $\lambda/4$ wave plate followed by another $\lambda/2$ wave plate. In this Letter, the peak laser intensity is fixed at 3×10^{11} W/cm^2, while the ellipticity is changed from 0 to 0.8. The ions and electrons are detected coincidentally, with their momentum vectors reconstructed in a way identical to the conventional cold-target recoil-ion momentum spectrometer. For a more comprehensive description of the experimental setup, please refer to Supplemental Material [31].

It is important to note that the polarization directions n_i $(i = 1, 2, \ldots, 6)$ of the excited electrons differ from the main axis of the system, which is chosen as the propagation direction y of the ionizing laser throughout the Letter. In the case of all six cooling lasers being turned on simultaneously, the excited Rb atoms are evenly populated in three magnetic sublevels of the $5p$ state, corresponding to m of 1, 0, and -1, respectively. Since we are interested in the momentum distribution on the polarization plane, the ionization of the initial state with $m = 0$ can be neglected [31]. The single-photon ionization pathways of the Rb $5p$ states driven by the elliptically polarized laser are illustrated in Fig. 1(b), where the Rb atoms are prepared in the $|1, 1\rangle_y$ (the subscript y specifies the quantization axis) and $|1, -1\rangle_y$ states, and the final states after single ionization are a superposition of $|0, 0\rangle_y$, $|2, 0\rangle_y$, $|2, 2\rangle_y$, and $|2, -2\rangle_y$.

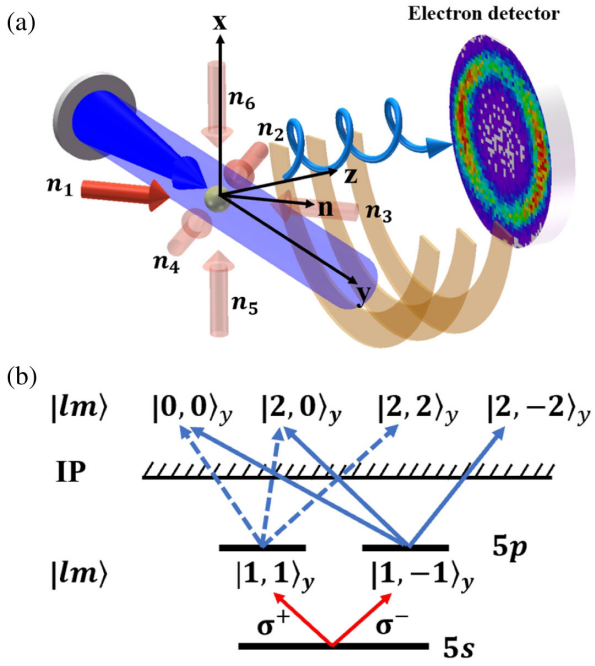

FIG. 1. (a) Experimental setup. The Rb atoms are cooled and excited by left-handed circularly polarized lasers at 780 nm (shown by the six red arrows) and then ionized by a femtosecond laser at 400 nm (shown by the blue arrow). The femtosecond ionizing laser propagates in the y direction and polarizes in the x-z plane. The six cooling laser beams are denoted by n_1–n_6, two of which are in the x direction, and four in the y-z plane spanning an angle of 45° with respect to the y axis. The three-dimensional momentum spectrum of the photoelectron is measured by a reaction microscope. (b) Excitation and ionization channels of the Rb atoms. The red arrow represents a 780 nm cooling laser to prepare the Rb atoms in an excited state. The ionization pathways from the $5p$ state with $m = 1$ and -1 are demonstrated by the blue dashed and solid arrows, respectively.

The ionization thresholds of the $5s$ and $5p$ state are 4.17 eV and 2.58 eV, respectively. When a 400 nm photon (3.1 eV) is absorbed by a Rb atom in the $5s$ state, the energy is insufficient for ionization, requiring at least the absorption of two photons to achieve ionization. The corresponding radial momentum of the photoelectron is

$p_r = \sqrt{p_x^2 + p_z^2} = 0.39$ a.u. On the other hand, the $5p$ state can be ionized by the absorption of a single photon resulting in the photoelectron radial momentum of 0.2 a.u. These two ionization channels can be easily distinguished in the momentum spectrum owing to the high resolution of the electron and ion detectors [29,32,39].

As a benchmark, we first perform a measurement with all six cooling laser beams turned on. Figure 2(a) shows a typical momentum spectrum measured at a peak intensity of 3×10^{11} W/cm^2, which is sufficiently low that two-photon ionization of the ground state is significantly suppressed. The 400 nm laser field is elliptically polarized, with its major axis located in the z direction, rotating anticlockwise, and the ellipticity is 0.5. It can be seen that the photoelectrons' most probable emission angle is along the major axis and remains unchanged over a wide range of laser intensities and ellipticities [31]. The time-dependent Schrödinger equation (TDSE) simulation shown in Fig. 2(b) confirms the experimental observation. This finding contrasts with previous observations in the multi-photon or tunneling ionization regime for hydrogen and noble gas atoms, where a notable angular offset is observed in a close-to-circularly polarized laser field and varies with the ellipticity [40]. The offset angle therein is of particular interest, often attributed to the Coulomb scattering of the photoelectron by the parent ion, as described by the Keldysh-Rutherford model.

Laser cooling offers the possibility to break down the symmetry, thereby providing a new possibility to achieve a well-designed *complete* photoionization measurement. For

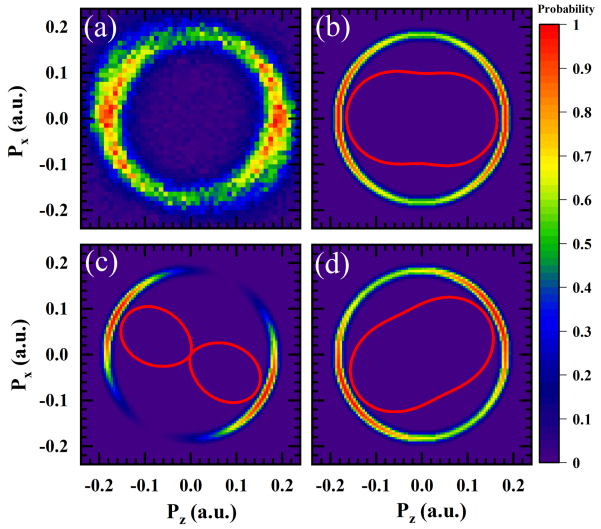

FIG. 2. Measured (a) and calculated (b) PMD of the $5p$ state in the p_x-p_z plane. (c) and (d) are the calculated results of the initial state $m = -1$ and 1, respectively. The red solid curves in (b)–(d) are the corresponding angular distributions. The laser intensity is 3×10^{11} W/cm^2. The elliptically polarized laser field rotates in the counterclockwise direction, with its major polarization axis in the z direction and an ellipticity of 0.5.

instance, if the Rb atom is polarized in the y dimension, as shown in Figs. 2(c) and 2(d) for the initial quantum states prepared in the $m = -1$ (polarized along the $-y$ axis) and $m = 1$ (polarized along the $+y$ axis) Zeeman sublevels, respectively, a notable angular offset in the photoelectron momentum distribution (PMD) is expected, similar to the previous observation as in Ref. [40]. Further studies show that the angular offset is entirely determined by the atomic potential [31], i.e.,

$$\varphi_{\max} = \pm\frac{1}{2}\operatorname{atan}\frac{2\sqrt{2}|D_s/D_d|\sin(\Delta\phi_C)}{1+2\sqrt{2}|D_s/D_d|\cos(\Delta\phi_C)}, \quad (1)$$

and does not change with the ellipticity or intensity of the external electric field. Here, $|D_d/D_s|$ is the ratio of the reduced electric dipole matrix elements from the $5p$ state to the ϵd and ϵs continua [38], and $\Delta\phi_C$ is the phase difference of the corresponding Coulomb wave functions, including both the short-range phase shift and the Coulomb phase shift. In this respect, the PMD does provide a chronoscope to clock the EWS time delay by mapping the phase information of the partial waves into the tilt angle of the PMD. However, since $\varphi_{\max}$ is a function of both $|D_d/D_s|$ and $\Delta\phi_C$, we cannot uniquely determine their exact values solely from $\varphi_{\max}$. Below we will provide an efficient way to disentangle these two parameters.

We choose to break the symmetry of the system by keeping only one beam of the cooling lasers on, e.g., n_1 [see Fig. 1(a)], while turning off all others. In this way, the Rb atom is polarized into the n_1 direction, which can be regarded as a superposition state of the $m = 1$ and $m = -1$ states after projecting to the quantization main axis y. Consequently, the final momentum spectrum is a coherent superposition of the results similar to that shown in Figs. 2(c) and 2(d) (but of course, for the linearly polarized field, shown in Supplemental Material [31]), that is,

$$|\mathcal{M}^{n_1}_{m=1}(\mathbf{p})|^2 = \left|\frac{2+\sqrt{2}}{4}\mathcal{M}^{y}_{m=1}(\mathbf{p}) + \frac{2-\sqrt{2}}{4}\mathcal{M}^{y}_{m=-1}(\mathbf{p})\right|^2. \quad (2)$$

Here, the coefficients are due to the coordinate transformation of the spherical harmonics [31]. Experimental measurement and the corresponding TDSE simulation are shown in Figs. 3(a) and 3(b), respectively. We then extract the photoelectron angular distributions (PADs) from the PMDs: for experiment, the radial momentum p_r is integrated from 0.175 a.u. to 0.195 a.u. (momentum resolution is approximately 0.02 a.u.) to ensure sufficient counts so as to reduce the statistical uncertainty and the result is shown as the black full circles in Fig. 3(c); for theory, the PAD is shown for $p_r = 0.185$ a.u. (radial peak of the PMD) as the black dashed line in Fig. 3(d). In both cases, two side lobes are observed in the second and fourth quadrants.

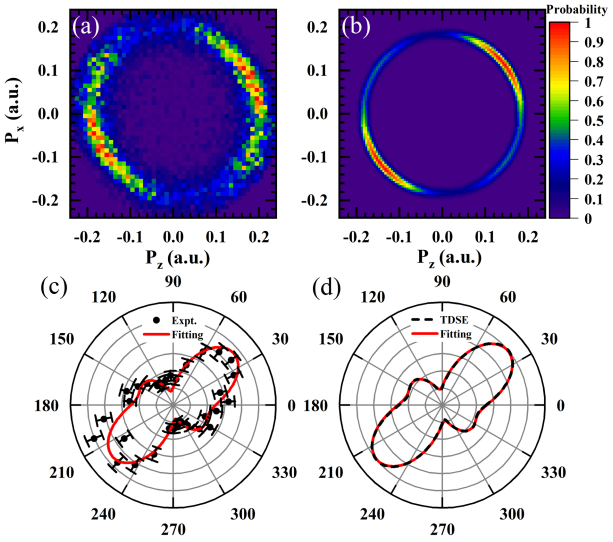

FIG. 3. Measured (a) and calculated (b) PMDs of the $5p$ state in the p_x-p_z plane with only one cooling laser beam retained (n_1, for example). The angular distributions extracted from experiment (a) and theory (b) are shown in (c) and (d), respectively. The laser parameters are the same as Fig. 2 but for a linearly polarized laser field.

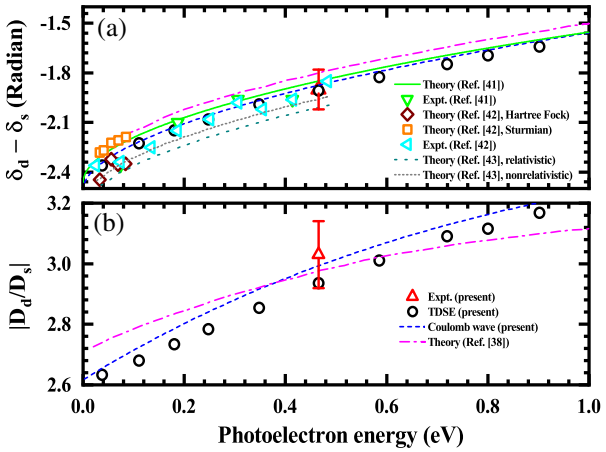

FIG. 4. The extracted continuum phase difference between ϵd and ϵs states (a) and the ratio of electric dipole matrix elements from $5p$ to these two partial waves (b) as a function of the photoelectron energy. The red triangles mark the experimental results, the black circles are TDSE simulations, and the blue dashed curves are calculated directly from the central field radial wave functions. These results are then compared with some early experimental data and theoretical predictions. The legends in (b) also apply to (a).

This additional interference-induced asymmetry, together with the most probable emission angle, provides the possibility to simultaneously determine the amplitudes and phases of the ionization channels.

To this end, we fit the experimentally measured PAD with the following formula:

$$|\mathcal{M}^{n_1}_{m=1}(\varphi)|^2 \propto \left|1+\frac{1}{2\sqrt{2}}\left|\frac{D_d}{D_s}\right|e^{i\Delta\phi_C} \times \left[1+3\sqrt{2}i\sin(2\varphi)+3\cos(2\varphi)\right]\right|^2, \quad (3)$$

which is obtained by perturbative analysis of the PAD [31]. The fitting result shown with the red line in Fig. 3(c) gives rise to $\Delta\phi_c = -1.90 \pm 0.12$ rad and $|D_d/D_s| = 3.03 \pm 0.11$. For the TDSE result fitted in the same way, as shown by the red line in Fig. 3(d), we get $\Delta\phi_c = -1.91$ rad and $|D_d/D_s| = 2.94$. Remarkable agreement between experiment and theory is achieved.

The above scheme is rather general and can be extended to other photoelectron energies by changing the wavelength of the ionizing laser. In this way, one can obtain an energy-dependent phase shift and study the EWS time delay. We demonstrate this possibility with further numerical simulations shown in Fig. 4. With the increase of the laser wavelength, the energy of emitted photoelectrons varies, and the phase difference between the partial waves changes accordingly. We show a comparison between the phase difference extracted from the TDSE results and the Coulomb wave functions calculated independently using different model potentials at different photoelectron energies. They are in good agreement with the results of Refs. [38,41–43] over the whole range of parameters. It is important to note that in some early measurements, such as those reported in Refs. [41,42], a distinct (two-photon nonresonant ionization) approach was utilized. In that scheme, all p states take part in the ionization pathways [43]. By comparison, we have adopted a two-color scheme and are able to target the intermediate state solely onto the $5p$ state. Both approaches reach the ϵs and ϵd partial waves, allowing for the extraction of both the phase difference and the amplitude ratio. While the phase difference extracted is consistent across both methods, the amplitude ratio is completely different due to their distinctly different quantum paths [44]. Our work not only demonstrates the new opportunity of quantum control but also facilitates a stringent test of the theory by a much cleaner ionization channel.

In summary, by taking full advantage of the flexibility offered by the laser cooling system in our MOTReMi platform, we can prepare laser-aligned $5p$ states and control their magnetic quantum number. We have proposed an intuitive method that directly extracts the phase difference of the final-state wave function and the transition amplitude of various ionization channels from the two-dimensional photoelectron momentum distribution. The scheme is rather robust in the sense that it is not sensitive to the ellipticity or intensity of the ionizing laser. It naturally avoids the complexity (additional phase shift or time delay) that might be introduced in popular pump-probe approaches [45–47], making the extraction more

straightforward. Moving ahead, our experimental method also paves the road to study the m-resolved transition dynamics and circular dichroism of photoelectrons on the attosecond time scale [48], and to resolve and control the interference between Zeeman sublevels [49], which are difficult for traditional RABBIT measurements where the XUV and IR pulses have parallel polarizations.

Acknowledgments—This work is supported by the National Natural Science Foundation of China (NSFC) (Grants No. 12334011, No. 12374262, No. 12174034, and No. 12474259) and the National Key Research and Development Program of China (Grant No. 2022YFA1604302). We also acknowledge support from the Shanghai-XFEL beamline project (SBP) (Grant No. 31011505505885920161A2101001).

[1] J. M. Dahlström, A. L'Huillier, and A. Maquet, J. Phys. B **45**, 183001 (2012).
[2] R. Pazourek, S. Nagele, and J. Burgdörfer, Rev. Mod. Phys. **87**, 765 (2015).
[3] L. Eisenbud, The formal properties of nuclear collisions, Ph.D. thesis, Princeton University, 1948.
[4] E. P. Wigner, Phys. Rev. **98**, 145 (1955).
[5] F. T. Smith, Phys. Rev. **119**, 2098 (1960).
[6] H. Kleinpoppen, B. Lohmann, and A. N. Grum-Grzhimailo, *Perfect/Complete Scattering Experiments* (Springer, Berlin, 2013).
[7] A. N. Grum-Grzhimailo and E. V. Gryzlova, in *Progress in Photon Science: Recent Advances*, edited by K. Yamanouchi, S. Tunik, and V. Makarov (Springer, Switzerland, 2019), Chap. 13, pp. 263–282.
[8] V. Schmidt, Rep. Prog. Phys. **55**, 1483 (1992).
[9] C. Heckenkamp, F. Schäfers, G. Schönhense, and U. Heinzmann, Z. Phys. D **2**, 257 (1986).
[10] C. Roth, F. U. Hillebrecht, H. B. Rose, and E. Kisker, Phys. Rev. Lett. **70**, 3479 (1993).
[11] A. Hausmann, B. Kämmerling, H. Kossmann, and V. Schmidt, Phys. Rev. Lett. **61**, 2669 (1988).
[12] M. Meyer, B. Müller, A. Nunnemann, T. Prescher, E. v. Raven, M. Richter, M. Schmidt, B. Sonntag, and P. Zimmermann, Phys. Rev. Lett. **59**, 2963 (1987).
[13] M. Pahler, C. Lorenz, E. v. Raven, J. Rüder, B. Sonntag, S. Baier, B. R. Müller, M. Schulze, H. Staiger, P. Zimmermann, and N. M. Kabachnik, Phys. Rev. Lett. **68**, 2285 (1992).
[14] A. von dem Borne, T. Dohrmann, A. Verweyen, B. Sonntag, K. Godehusen, and P. Zimmermann, Phys. Rev. Lett. **78**, 4019 (1997).
[15] O. Plotzke, G. Prümper, B. Zimmermann, U. Becker, and H. Kleinpoppen, Phys. Rev. Lett. **77**, 2642 (1996).
[16] K. Godehusen, P. Zimmermann, A. Verweyen, A. von dem Borne, P. Wernet, and B. Sonntag, Phys. Rev. A **58**, R3371 (1998).
[17] M. Meyer, A. N. Grum-Grzhimailo, D. Cubaynes, Z. Felfli, E. Heinecke, S. T. Manson, and P. Zimmermann, Phys. Rev. Lett. **107**, 213001 (2011).
[18] P. A. Carpeggiani, E. V. Gryzlova, M. Reduzzi, A. Dubrouil, D. Facciala, M. Negro, K. Ueda, S. M. Burkov, F. Frassetto, F. Stienkemeier, Y. Ovcharenko, M. Meyer, O. Plekan, P. Finetti, K. C. Prince, C. Callegari, A. N. Grum-Grzhimailo, and G. Sansone, Nat. Phys. **15**, 170 (2019).
[19] P. B. Corkum and F. Krausz, Nat. Phys. **3**, 381 (2007).
[20] F. Krausz and M. Ivanov, Rev. Mod. Phys. **81**, 163 (2009).
[21] M. Hentschel, R. Kienberger, C. Spielmann, G. A. Reider, N. Milosevic, T. Brabec, P. Corkum, U. Heinzmann, M. Drescher, and F. Krausz, Nature (London) **414**, 509 (2001).
[22] J. Itatani, F. Quéré, G. L. Yudin, M. Y. Ivanov, F. Krausz, and P. B. Corkum, Phys. Rev. Lett. **88**, 173903 (2002).
[23] M. Schultze *et al.*, Science **328**, 1658 (2010).
[24] P. M. Paul, E. S. Toma, P. Breger, G. Mullot, F. Augé, P. Balcou, H. G. Muller, and P. Agostini, Science **292**, 1689 (2001).
[25] K. Klünder, J. M. Dahlström, M. Gisselbrecht, T. Fordell, M. Swoboda, D. Guénot, P. Johnsson, J. Caillat, J. Mauritsson, A. Maquet, R. Taïeb, and A. L'Huillier, Phys. Rev. Lett. **106**, 143002 (2011).
[26] M. Isinger, R. J. Squibb, D. Busto, S. Zhong, A. Harth, D. Kroon, S. Nandi, C. L. Arnold, M. Miranda, J. M. Dahlström, J. M. Dahlström, E. Lindroth, R. Feifel, M. Gisselbrecht, and A. L'Huillier, Science **358**, 893 (2017).
[27] J. Peschel, D. Busto, M. Plach, M. Bertolino, M. Hoflund, S. Maclot, J. Vinbladh, H. Wikmark, F. Zapata, E. Lindroth, M. Gisselbrecht, J. M. Dahlstroem, A. L'Huillier, and P. Eng-Johnsson, Nat. Commun. **13**, 5205 (2022).
[28] D. Fischer, D. Globig, J. Goullon, M. Grieser, R. Hubele, V. L. B. de Jesus, A. Kelkar, A. LaForge, H. Lindenblatt, D. Misra, B. Najjari, K. Schneider, M. Schulz, M. Sell, and X. Wang, Phys. Rev. Lett. **109**, 113202 (2012).
[29] H. Ma, X. Wang, L. Zhang, Z. Zou, J. Yuan, Y. Ma, R. Lv, Z. Shen, T. Yan, M. Weidemüller, D. Ye, and Y. Jiang, Phys. Rev. A **107**, 033114 (2023).
[30] We have also tried to solve the time-dependent Schrödinger equation incorporating spin-orbit coupling and confirmed that the main results presented in this Letter, including Figs. 2–4, are almost identical with or without the inclusion of spin-orbit coupling. Therefore, the fine structure effects can be safely neglected in the present study. A detailed report of the numerical recipes dealing with spin-orbit coupling in strong laser fields and its application to the studies of rare-gas atoms with large fine structure effects (spin-orbit splitting $>$ leV) will be given elsewhere.
[31] See Supplemental Material at http://link.aps.org/supplemental/10.1103/PhysRevLett.134.123204 for more details on the experimental setup, methodology of *ab initio* simulations, theoretical analysis of the photoelectron angular distributions, and more results on the photoelectron momentum distributions, which includes Refs. [32–38].
[32] R. Y. Li, J. Y. Yuan, X. C. Wang, X. Y. Hou, S. Zhang, Z. Y. Zhu, Y. X. Ma, Q. Gao, Z. Y. Wang, T. M. Yan, C. C. Qin, S. Li, Y. Z. Zhang, M. Weidermüller, and Y. H. Jiang, J. Instrum. **14**, P02022 (2019).
[33] A. L'Huillier, L. A. Lompré, G. Mainfray, and C. Manus, J. Phys. B **16**, 1363 (1983).
[34] W. Schweizer, P. Faßbinder, and R. González-Férez, At. Data Nucl. Data Tables **72**, 33 (1999).

[35] X. M. Tong and S. I. Chu, Chem. Phys. **217**, 119 (1997).
[36] X. Wu, Z. Yang, S. Zhang, X. Ma, J. Liu, and D. Ye, Phys. Rev. A **103**, L061102 (2021).
[37] L. B. Madsen, L. A. A. Nikolopoulos, T. K. Kjeldsen, and J. Fernández, Phys. Rev. A **76**, 063407 (2007).
[38] I. D. Petrov, V. L. Sukhorukov, E. Leber, and H. Hotop, Eur. Phys. J. D **10**, 53 (2000).
[39] J. Yuan, S. Liu, X. Wang, Z. Shen, Y. Ma, H. Ma, Q. Meng, T.-M. Yan, Y. Zhang, A. Dorn, M. Weidemüller, D. Ye, and Y. Jiang, Phys. Rev. A **102**, 043112 (2020).
[40] D. Trabert, N. Anders, S. Brennecke, M. S. Schöffler, T. Jahnke, L. P. H. Schmidt, M. Kunitski, M. Lein, R. Dörner, and S. Eckart, Phys. Rev. Lett. **127**, 273201 (2021).
[41] Z.-M. Wang and D. S. Elliot, Phys. Rev. Lett. **84**, 3795 (2000).
[42] Z.-M. Wang and D. S. Elliott, Phys. Rev. A **62**, 053404 (2000).
[43] J. Colgan and M. S. Pindzola, Phys. Rev. Lett. **86**, 1998 (2001).
[44] K. L. Ishikawa and K. Ueda, Phys. Rev. Lett. **108**, 033003 (2012).
[45] J. Fuchs, N. Douguet, S. Donsa, F. Martin, J. Burgdörfer, L. Argenti, L. Cattaneo, and U. Keller, Optica **7**, 154 (2020).
[46] C. Cirelli *et al.*, Nat. Commun. **9**, 955 (2018).
[47] M. Kotur, D. Guenot, A. Jimenez-Galan, D. Kroon, E. W. Larsen, M. Louisy, S. Bengtsson, M. Miranda, J. Mauritsson, C. L. Arnold, S. E. Canton, M. Gisselbrecht, T. Carette, J. M. Dahlstrom, E. Lindroth, A. Maquet, L. Argenti, F. Martin, and A. L'Huillier, Nat. Commun. **7**, 10566 (2016).
[48] M. Han, J.-B. Ji, T. Balčiūnas, K. Ueda, and H. J. Wörner, Nat. Phys. **19**, 230 (2022).
[49] W. Jiang, G. S. J. Armstrong, L. Han, Y. Xu, Z. Zuo, J. Tong, P. Lu, J. M. Dahlström, K. Ueda, A. C. Brown, H. W. van der Hart, X. Gong, and J. Wu, Phys. Rev. Lett. **131**, 203201 (2023).